The THEMIS Mission

V. Angelopoulos

Abstract The Time History of Events and Macroscale Interactions during Substorms (THEMIS) mission is the fifth NASA Medium-class Explorer (MIDEX), launched on February 17, 2007 to determine the trigger and large-scale evolution of substorms. The mission employs five identical micro-satellites (hereafter termed "probes") which line up along the Earth's magnetotail to track the motion of particles, plasma and waves from one point to another and for the first time resolve space–time ambiguities in key regions of the magnetosphere on a global scale. The probes are equipped with comprehensive in-situ particles and fields instruments that measure the thermal and super-thermal ions and electrons, and electromagnetic fields from DC to beyond the electron cyclotron frequency in the regions of interest. The primary goal of THEMIS, which drove the mission design, is to elucidate which magnetotail process is responsible for substorm onset at the region where substorm auroras map ($\sim$10 R_E): (i) a local disruption of the plasma sheet current (current disruption) or (ii) the interaction of the current sheet with the rapid influx of plasma emanating from reconnection at $\sim$25 R_E. However, the probes also traverse the radiation belts and the dayside magnetosphere, allowing THEMIS to address additional baseline objectives, namely: how the radiation belts are energized on time scales of 2–4 hours during the recovery phase of storms, and how the pristine solar wind's interaction with upstream beams, waves and the bow shock affects Sun–Earth coupling. THEMIS's open data policy, platform-independent dataset, open-source analysis software, automated plotting and dissemination of data within hours of receipt, dedicated ground-based observatory network and strong links to ancillary space-based and ground-based programs. promote a grass-roots integration of relevant NASA, NSF and international assets in the context of an international Heliophysics Observatory over the next decade. The mission has demonstrated spacecraft and mission design strategies ideal for Constellation-class missions and its science is complementary to Cluster and MMS. THEMIS, the first NASA micro-satellite constellation, is a technological pathfinder for future Sun-Earth Connections missions and a stepping stone towards understanding Space Weather.

V. Angelopoulos (✉)
IGPP/ESS UCLA, Los Angeles, CA 90095-1567, USA
e-mail: vassilis@ucla.edu

1 Introduction

A substorm is an avalanche of small-scale magnetotail energy surges (Lui et al. 2001) feeding from solar wind energy previously stored in the magnetotail lobes. During its course, auroral arcs intensify, move poleward and break up into smaller formations (Akasofu 1976). Substorms are ubiquitous at all solar phases and appear within all types of magnetospheric responses to solar wind input: Embedded within large storms they influence storm development (Daglis et al. 2000) and geo-effectiveness (Siscoe and Petschek 1997). They bind the beginning and end phases of magnetospheric convection bays (Sergeev et al. 1996a) and are closely related to pseudo-breakups (Aikio et al. 1999). Understanding the substorm process is a prerequisite to understanding the geo-magnetospheric response to all levels of solar wind energy throughput. However, the objective of deciphering the mechanism of substorm instability transcends its geophysical interest. It relates intimately to broader scientific questions, because it addresses basic plasma physics processes, such as cross-scale coupling between MHD and kinetic plasma instabilities (Shinohara et al. 2001; Voronkov et al. 1999). Beyond purely scientific applications are matters of more practical value to society, related to space weather processes (such as storms), which affect satellite communications and ground electrical distribution, and are inextricably linked to substorms. In summary, *substorms represent a fundamental mode of global magnetospheric circulation, a macroscopic instability whose phenomenological and theoretical understanding is crucial for space science, basic plasma physics and space weather.*

A substorm has well-demarcated global evolutionary phases corresponding to unique stages of the instability of the coupled solar wind-magnetospheric circulation of energy and magnetic flux. These unique stages include energy storage (growth phase), explosive release (onset) and eventual ionospheric dissipation (late expansion and recovery phases). Thus a substorm represents a fundamental mode of global circulation of energy and magnetic flux transport throughout Geospace. This global, macroscopic instability is as central to space physics and space weather as the extratropical cyclone is to meteorology and weather. Despite the elemental nature of the substorm process, the lack of appropriate spacecraft conjunctions from previous missions resulted in a contentious set of theories for its description. The question is not simply which is the operant plasma micro-instability at onset. Rather, even the location, onset time, extent and motion of the magnetotail energization process leading to the macroscopic substorm phenomenon are still unknown (Spence 1996).

Resolving the substorm problem requires accurate timing of three disparate but well-defined processes: ground auroral onset, current disruption onset at 8–10 R_E and reconnection onset at 20–30 R_E. Since these processes expand rapidly with time, knowledge of the onset location is as important as timing. THEMIS is the first mission specifically designed to determine the onset and evolution of the substorm instability. Towards this primary objective, THEMIS utilizes tail-alignments (conjunctions) between 5 identical probes on near-equatorial orbits, with periods that are multiples of each other.
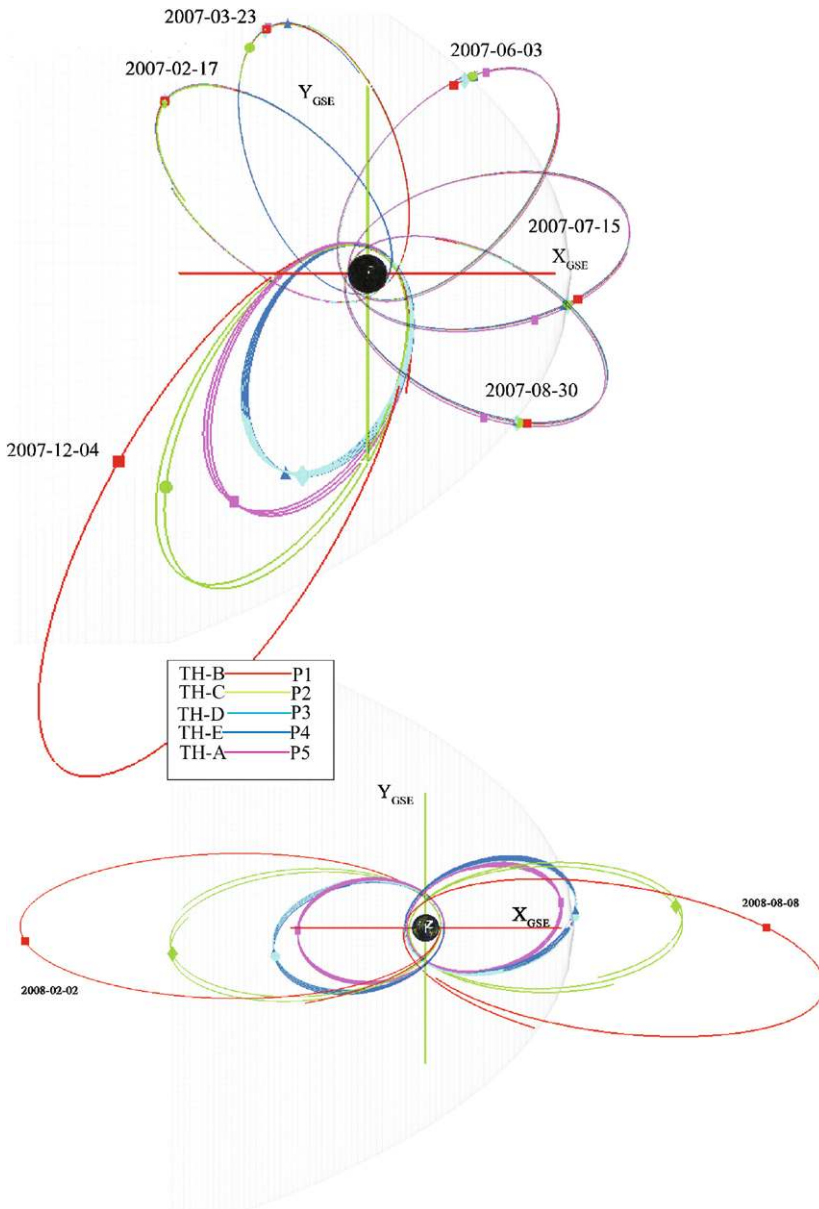
THEMIS has a two-year design life, mainly driven by its radiation environment (Harvey et al. 2008), and 100% total ionization dose margin; but due to a launch vehicle delay it was launched just past the center-tail encounter of 2007. To ensure that baseline objectives

remain intact and avoid a radical mission redesign late into the program, a post-launch coast-phase was prefixed to the baseline mission, giving it a total duration of 29 months. The tail mission phases last from early January to late-March in 2008 and in 2009. Radiation belt science objectives are addressed by the frequent probe traversals of the radiation belts on orbits whose periods and mean anomalies are dictated by the desire to align them in the tail. Natural evolution of the orbits in a Sun–Earth aligned system brings the probes to the dayside six months later, where THEMIS is able to address its dayside science objectives with a similar orbit strategy as in the tail. Thus, both dayside and radiation belt objectives are achieved with a mission design that is driven mainly by the tail science.

Table 1 describes the THEMIS science objectives. The THEMIS science and science closure is described in Sect. 2, and expanded upon in Sibeck et al. (2008). The THEMIS mission design is described in Sect. 3 and expanded upon in Frey et al. (2008). Figure 1 shows the orbital configurations during the first year of the baseline THEMIS mission. In the tail, reconnection is monitored by probes P1 (4 day period, $\sim$30 R_E apogee) and P2 (2 day period, $\sim$19 R_E apogee); while current disruption is monitored by probes P3 and P4 (1 day period, $\sim$12 R_E apogee). Four probes are required to accomplish the minimum mission (goals G1, G2 in Table 1); the fifth probe, P5, also on an approximately near-day period orbit, is an on-orbit spare that enhances mission reliability, but under nominal operations is used to perform timing and measure spatial gradients in yet one more dimension than would otherwise be possible with only two probes at the inner edge of the plasma sheet. Thus the fifth probe is required to satisfy other baseline requirements listed in Table 1, but is not required for the minimum mission. A network of ground observatories over the North American continent (from Eastern Canada to Western Alaska) monitors the aurora and space currents with white-light all-sky imagers and magnetometers, to provide accurate substorm onset timing, and is described in Mende et al. (2008). Probe alignments are designed to occur

Table 1 THEMIS science objectives

Mission driver	Science objective	Science goal
Primary	At the magnetotail: Onset and evolution of substorm instability	**G1** Time history of auroral breakup, current disruption, and lobe flux dissipation at the substorm meridian by timing:
		• Onset time of auroral breakup, current disruption and reconnection within <10 s.
		• Ground onset location within 0.5° in longitude and in space within 1 R_E.
		G2 Macroscale interaction between current disruption and near-Earth reconnection.
		G3 Coupling between the substorm current and the auroral ionosphere.
		G4 Cross-scale energy coupling between the macroscale substorm instability and local processes at the current disruption site.
Secondary	At radiation belts: Production of storm-time MeV electrons	Source and acceleration mechanism of storm-time MeV electrons.
Tertiary	At dayside: Control of solar wind-magnetosphere coupling by upstream processes	The nature, extent and cause of magnetopause transient events.

Fig. 1 *Top*: THEMIS coast phase actual orbits; *Bottom*: THEMIS 1st year baseline orbit predicts. (Axis size is 10 R$_E$)

year-round over the same point on the ground, i.e., over the North American sector. For the tail phase this corresponds to conjunctions between 00:30UT and 12:30UT and for the dayside it corresponds to conjunctions approximately 12 hrs later each day. This approach also optimizes utilization of GOES satellite magnetometer data sets and ground-based assets in North America.

THEMIS's five identical probes are equipped with five instruments each, measuring ions and electrons from ∼5 eV to ∼1 MeV and electromagnetic waves from DC to > 4 kHz. The instruments are summarized in Sect. 4 and are individually expanded upon in separate papers within this issue. Mission operations are performed by the Mission Operations Center (MOC) at SSL/UCB, as summarized in Sect. 5 and expanded upon in Bester et al. (2008). Science operations, data processing and analysis software is also summarized in Sect. 5 and expanded upon in Phan et al. (2008). All instruments and spacecraft are operating nominally and are expected to last for many years past their nominal lifetime. Plans for an extended mission are currently under way.

2 Science Objectives

Previous missions and fortuitous spacecraft conjunctions have provided a wealth of information regarding the substorm process but have been unable to determine where and how the substorm instability starts because of their un-optimized vantage points. Previous missions and fortuitous spacecraft conjunctions have been unable to determine where and how the substorm instability starts because of their unoptimized vantage points. For example, POLAR-Cluster radial conjunctions in the near-Earth plasma sheet result in less than 30 hrs of plasma sheet observations in rough Sun–Earth alignment, during which only a couple of times the near-neutral sheet location is sampled by both spacecraft. Geotail plasma sheet observations from 30 R_E in conjunction with inner magnetospheric probes (e.g., LANL satellites) results in significant observation time of substorms but without a satellite at the inner edge of the plasma sheet, where current disruption is expected to initiate. What is needed therefore is a dedicated multisatellite mission to measure with common instrumentation and with prolonged residence in the plasma sheet at 10, 20 and 30 R_E the process of current disruption and reconnection and their relative timing, as well as relationship to ground onset. THEMIS answers that need. This section is an outline of the key scientific objectives of the THEMIS mission that affect mission requirements.

2.1 Primary Objective: Substorm Causality

The components of the substorm instability i.e., Auroral Break-up, Current Disruption and Reconnection, evolve on a meso-scale range but interact over macroscales. High-sensitivity all sky imagers (ASIs) show (Friedrich et al. 2001) that the pre-onset equatorward arcs undergo large-scale undulations with wavelengths of hundreds of kilometers (Fig. 2). This is ∼6° in longitude, which maps to a region of $\delta Y \sim 1$ R_E at the inner edge of the plasma sheet. Onset erupts in 10 s at a folding of one such undulation.

An intense cross-tail current (Lui 1996) (tens of nA/m^2), mainly supported by a duskward anisotropy in thermal ions (2–10 keV), provides substantial free energy at growth phase at ∼10 R_E. At substorm onset the *current wedge* forms there (McPherron et al. 1973). This is an abrupt increase in the Z_{GSM} component of the magnetic field, accompanied by plasma heating. This morphological change of the field (Fig. 3) is consistent with a current-carrying particle distribution change (Mitchell et al. 1990). A current wedge is modeled as a partial disruption of the cross-tail current and diversion *along* the field lines, *into* the auroral ionosphere (Atkinson 1967; McPherron et al. 1973) where it feeds into the break-up arc. It is often termed the current disruption (CD) process (Lui et al. 1988). The hot, dipolar plasma originates in a small (Ohtani et al. 1991) equatorial area (∼1 R_E^2) and expands azimuthally (Nagai 1982) up to ∼10° of magnetic local time (MLT) per min and radially (Jacquey et al. 1991; Ohtani et al. 1992a, 1992b) at ∼200 km/s.
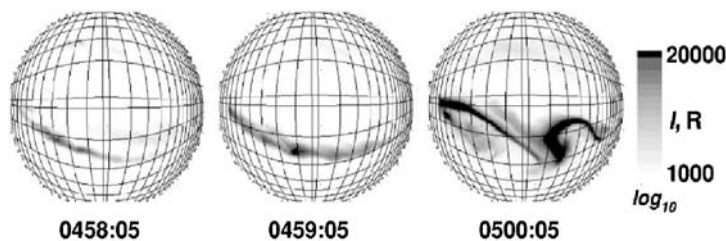
Fig. 2 Substorm onset as seen from a ground all sky camera station (Friedrich et al. 2001). Each line is 0.5 degrees in latitude (or 56 km) and in longitude (or 31 km)

Fig. 3 Development of the substorm current wedge through a reduction of the cross-tail current at 8–10 R_E in the equatorial plasma sheet
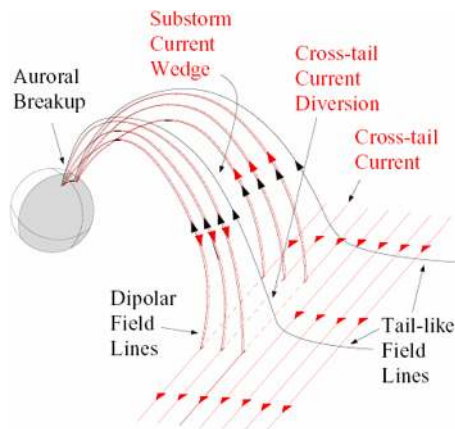
Further downtail, at ∼25 R_E, there is evidence that *magnetic reconnection* takes place (Nagai et al. 1998). Fast, bursty, bulk ion flows presumably emanating from the reconnection site at Earthward speeds comparable to the Alfven velocity (1000 km/s), are also interpreted (Hones 1976; Nagai et al. 1997) as evidence of that process. Seen as close to Earth as 10 R_E (Fairfield et al. 1998, Angelopoulos et al. 1999) such flows are often localized to within 1–3 R_E (Sergeev et al. 1996b; Angelopoulos et al. 1997a) but are very efficient in energy and flux transport (Angelopoulos et al. 1994).

Presently, all possible causal sequences involving auroral break-up, Rx onset, CD onset and external triggers are viable hypotheses (Kennel 1992). In particular, CD and Rx might be causally linked, or may proceed independently of each other. As an impartial and experienced researcher summarizes:

"Observations are gradually leading to a coherent picture of the interrelations among these various onset phenomena, but their cause remains a controversial question. The abrupt nature of substorm onsets suggests a magnetospheric instability, but doubt remains as to its nature and place of origin. Measurements increasingly suggest the region of 7–10 R_E near midnight as the likely point of origin" (Fairfield et al. 1992).

A number of substorm onset paradigms exist, but two of them can help epitomize the main ideas and reveal the primary observational requirements. These are the *"current disruption"* and the *"Near-Earth Neutral Line" (NENL)* paradigms.

According to the current disruption paradigm, an instability *local* to the current disruption region (8–10 R_E) is responsible for substorm onset (Lui 1996). The paradigm stems from two

Fig. 4 Time-history of events at the substorm meridian according to the Current Disruption model for substorms (adapted from Lui 1991). *Numbers* indicate proposed chronological and causal sequence
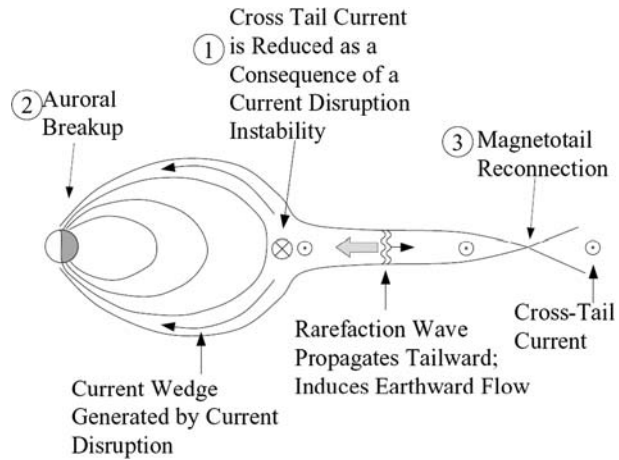
Table 2 CD model event chronology

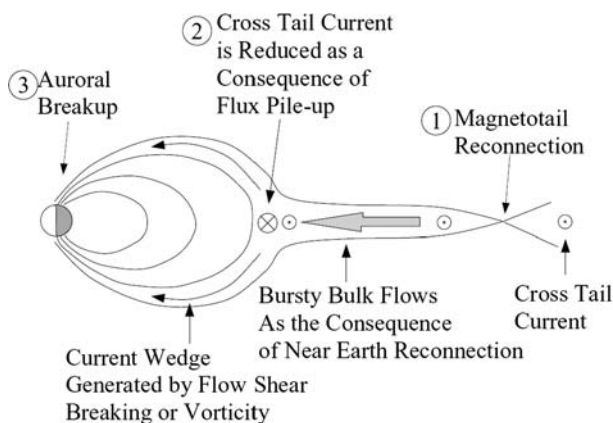| Order	Time (s)	Event
1	$t = 0$	Current disruption
2	$t = 30$	Auroral breakup
3	$t = 60$	Reconnection

basic observations: First, the break-up arc maps near Earth (Lui and Burrows 1978). This has been reinforced through advanced mapping of auroral images from Viking (Elphinstone et al. 1995), POLAR (Frank et al. 1998; Frank and Sigwarth 2000) and by ground-based observations (Samson 1992; Voronkov et al. 1999). Second, the cross-tail current density reaches tens of nA/m^2 and peaks near 8–10 R$_E$ prior to substorm onset (Kaufmann 1987). This happens explosively (Ohtani et al. 1992a, 1992b) suggesting that it is in *that* region that the free-energy source and trigger for the substorm auroral surges reside. This paradigm suggests (Fig. 4) that Rx and fast Earthward flows are triggered by a CD-initiated fast mode rarefaction wave ($V_x = -1600$ km/s) once it reaches ~25 R$_E$. Flows cause neither the CD nor the auroral break-up itself. This rarefaction wave has not been conclusively reported before, as natural plasma sheet oscillations and the resultant diamagnetic effect, cause large amplitude, background magnetosonic waves. The relevant substorm component chronology appears in Table 2.

Recent experimental evidence in support of this paradigm comes from the observation that the particles energized first at the CCE spacecraft (located at 8–9 R$_E$) at onset are those with gyrocenters Earthward of CCE (Lui et al. 1988; Ohtani 1998). Finite gyroradius remote sensing applied on equatorial pitch angles produces the CD expansion's speed and direction ($\mathbf{V}_{xy}$). However, performing accurate CD onset timing requires knowledge of the CD expansion velocity at two probes which bracket the onset location. The probes should be at the neutral sheet (± 2 R$_E$) and near the CD location itself (± 2 R$_E$) so that the expansion speed will not vary significantly during its motion. Such timing has not been performed to date.

According to the Near Earth Neutral Line (NENL) paradigm (Hones 1976; Baker et al. 1996), bursty flows generated by near-Earth reconnection (Baumjohann et al. 1989) (~ 25 R$_E$) are responsible for substorm onset (Fig. 5). Observations pivotal for this model's development at the substorm meridian include fast tailward/Earthward flows (Hones 1976;

Fig. 5 Similar to Fig. 4, but from the viewpoint of the NENL model for substorms (adapted from Shiokawa et al. 1998b). Note the difference in the sequence of events

Table 3 NENL model event chronology

Order	Time (s)	Event
1	$t = 0$	Reconnection
2	$t = 90$	Current disruption
3	$t = 120$	Auroral breakup

Nagai et al. 1997) and plasmoid ejection (Hones et al. 1984; Slavin et al. 1992) both timed
to start within 1–2 minutes from ground onset. This paradigm suggests that the flow kinetic
energy is converted to particle thermal energy at the CD region. While heating generates a
steep pressure gradient, the flow decelerates and deflects around Earth. The field-aligned cur-
rent created locally by these processes (Hesse and Birn 1991; Shiokawa et al. 1998a, 1998b;
Birn et al. 1999) leads to current disruption and auroral breakup. The recent observation that
fast Earthward flows at 12–18 R_E occur within 1 min from substorm onset (Angelopoulos
et al. 1997b; Shiokawa et al. 1998a, 1998b; Sergeev et al. 1995; Petrukovich et al. 1998;
Yamade et al. 2000) has spurred renewed interest in field-aligned current generation in the
NENL context. The NENL substorm component chronology differs from the current disrup-
tion model's (Table 3).

The NENL-predicted fast flow protrusion at 8–10 R_E has been rarely reported at sub-
storm onset, but has been seen during pseudo-breakups, auroral streamer events (Hender-
son et al. 1998; Sergeev et al. 2000) and at substorm recovery (Nakamura et al. 2001a,
2001b). This has led to the suggestion (Ohtani 2001) that pseudo-breakup flows are CD
onset triggers/substorm precursors. Alternatively: (i) The incoming flow may decelerate to
compensate for the increasing magnetic field (Schodel et al. 2001) or (ii) The flow may
dissipate through field-aligned Poynting flux (Wygant et al. 2000) along high latitude field
lines (Zesta et al. 2000; Angelopoulos et al. 2001). The flow evolution and causal relation-
ship (if any) to substorm onset is unclear, largely due to a lack of tail-aligned spacecraft
conjunctions.

As in the case of CD onset detection, accurate Rx onset timing requires *two* probes at
the plasma sheet, or its boundary, measuring velocity dispersed, field aligned, 30–300 keV
particles. A strictly temporal interpretation of the dispersion provides L, the distance to the
source (Sarris et al. 1976, 1996). A spatial interpretation (Richardson et al. 1987; Richardson
and Cowley 1985) provides $L \cdot V_E / V_B$. Here, V_E is the convection velocity along the flight

path of the particles (inferred by the dawn-dusk electric field component or measured by the plasma detector). V_B is the Z_{GSM} component of the boundary velocity measured by finite gyroradius remote sensing on East–West particle fluxes. The latter is the more general interpretation (when $V_E = V_B$ we retrieve the temporal one), but can only be used if the Rx site is nearby (within ∼5–10 R_E), because the locally measured V_E / V_B is not necessarily constant along distant flight paths. Thus two probes at distances of 5–10 R_E from each other should *bracket* the nominal Rx site. Oppositely-directed fluxes at the probes establish that the reconnection site is between them (nearby), justifying the assumption of a constant V_E / V_B. The two probes should observe the particles as the boundary expands over. Thus the two Rx monitors need not be at the neutral sheet but within $\delta Z_{GSM} \sim 5\, R_E$ of it. Plasma sheet Z-fluctuations affect little the timing capability because the active plasma sheet expansions are large relative to those fluctuations. Such accurate Rx timing has not been performed to date.

Distinguishing between the CD and NENL models imposes similar observational requirements on timing and location as distinguishing between all substorm models. For example the Magnetosphere-Ionosphere (MI) coupling model (Kan 1998) suggests that the substorm starts due to the breaking of the Earthward flows at a rate >3 mV/m/R_E, and the ensuing Alfven wave bouncing. Contrary to the current disruption model, the flows come first, as a result of mid-tail or distant tail processes and the remaining sequence of events is similar to the current disruption scenario. As in the current disruption model, Rx is not a necessary condition for onset triggering.

Spontaneous (Henderson et al. 1996) onsets and externally triggered (McPherron et al. 1986; Lyons 1996) onsets (stimulated by sudden impulses, northward turnings or rotational discontinuities (Sergeev et al. 1990)) may exhibit different destabilization scenarios (Lyons 1995). It is possible, e.g., that external triggers result in an NENL-like path to substorm onset, whereas spontaneous onset substorms follow the CD paradigm prescription. It is thus important to classify substorms according to the external conditions in order to distinguish between different scenarios.

The science goals and objectives of Table 1, and the previous discussion on substorm phenomenology lead to a set of Mission Requirements (MR). These requirements are tabulated in Table 4. For example, ground onset timing should be performed along the substorm onset meridian ($\delta MLT \sim 6°$, which corresponds to 1 R_E at the CD site) and must be better than the time scale of interaction of those processes (30 s). Since CD onset is limited in $\delta XY \sim 1\, R_E^2$ the CD monitors should be no more than $\delta Y \sim \delta X \sim \pm 2\, R_E$ apart. Rx monitors should be around 19 R_E and 30 R_E, i.e., within $\pm 5\, R_E$ of the nominal Rx site to ensure constancy of the measured V_E / V_B ratio. The neutral sheet location (maximum Z_{GSM} distance in winter solstice) determines the orbit inclination of both the CD and the Rx monitors. Diurnal fluctuations at 10 R_E ($\delta Z \pm 2\, R_E$) have little effect on the capability of the CD monitors to determine CD expansion speeds. Plasma sheet diurnal fluctuations at 20 and 30 R_E ($\delta Z \pm 3\, R_E$) are small compared to the $\pm 5\, R_E$ tolerance. Additionally, the two inner probes in combination should permit cross-tail ($\delta Y \sim 0.5$–$5\, R_E$) or cross-sheet ($\delta Z \sim 1\, R_E$) conjunctions (not necessarily simultaneously).

Mission Closure of these requirements is shown at the right-hand column of Table 4. The objective to time auroral onset using < 30 s time resolution ASIs in Alaska/Canada necessitates that the probe apogees are in the US winter season, at central US midnight, i.e., ∼6:30 UT (best performance of ASIs is in winter). This in turn calls for orbit periods that are multiples of a day. Remote sensing requirements for both CD and Rx monitors necessitate that they reside in near-equatorial orbits. Benign attitude Control System (ACS) requirements (better than 11.25°) are derived from the SST technical specifications (to control the

Table 4 THEMIS mission requirements and capability

Goal	Baseline [minimum] requirement	Mission capability
G1. Time history of breakup, CD, Rx at the substorm onset meridian	**MR1i** An ASI, two (a high- and a mid-latitude) GMAG stations per MLT hr, spin-point onset at δMLT < 1°, t_{res} < 30 s [one GMAG, δMLT < 6°].	**MC1i** 2 ground ASIs, 2 (high lat./mid lat.) magnetometers provide onset detection within δMLT < 0.5°, $δt = 1$ s. Even when cloudy, PiBs provide $δt = 1$ s and mid-lat. gmags determine onset meridian within δMLT < 5°.
	MR1ii 2 equatorial probes at 10 R_E, separated by $δXY \sim 2\ R_E$ monitor CD onset at t_{res} < 30 s [same].	**MC1ii** P3 & P4 ($δXY \sim 2\ R_E$) time CD onset at t_{res} < 10 s.
	MR1iii Two orbits bracketing Rx region, separated by $δY \sim 2\ R_E$ and at apogee within 5 R_E of neutral sheet (at 19 R_E, inc ~9° and at 30 R_E, inc ~7°) measure reconnection onset at t_{res} < 30 s [same].	**MC1iii** P1 & P2 at required orbits time once per 4 days at $δY \sim 2\ R_E$ ($δX \sim 6$–10 R_E) fast flow onset at t_{res} < 10 s.
	MR1iv CD and Rx monitors align (within ±2 R_E) during > 10 [>5] substorms near winter (±2 mo.).	**MC1iv** P1, P2, P3 & P4 align once per 4 days. P5 also part of alignment strategy (average ~12 hours/alignment). 80 substorms/yr; 16 substorm-alignments/yr).
	MR1v SST to measure on ecliptic plane (axis control ~ ± 30°) i^+/e^- fluxes (40–100 keV) at $t_{res} = 10$ s [same].	**MC1v** Spin-plane-mounted SST (20 keV to >1 MeV) on all probes at $t_{res} = 3$ s, covers required FOV at all seasons. Spin axis normal to ecliptic. ACS control~0.5°.
	MR1vi $δB/B \sim 10\%$, or $δB \sim 1$ nT absolute [same].	**MC1vi** $δB \sim 0.6$ nT absolute, routinely at 4 vectors/s.
G2. CD–Rx coupling.	**MR2i** Track rarefaction wave (1600 km/s) in B.	**MC2i, 2 ii** P3 & P2 measure time delays at $δX/δt = 6\ R_E/3$ s = 12000 km/s during 160 substorms (32-alignments)/yr.
	MR2ii Track earthward flows (400 km/s) in V.	
	MR2iii $δB \sim 1$ nT absolute, $δV/V \sim 10\%$.	**MC2iii** $δB \sim 0.6$ nT absolute and $δV/V \sim 10\%$.

Table 4 (*Continued*)

Goal	Baseline [minimum] requirement	Mission capability
G3. Substorm coupling to auroral ionosphere	**MR3i** Measure radial/cross-sheet pressure gradients ($\delta P/\delta XY \sim 0.1$ nPa/R_E); flow vorticity/deceleration ($\delta V/\delta XY \sim 100$ km/s R_E). Requires 10% accuracy in δV, δP over 1 R_E scales ($\delta P/P \sim \delta V/V \sim 1$).	**MC3i** δXY conjunctions between P3, P4, P5 over ranges of 0.3–10 R_E provide δP, δV with 10% absolute accuracy. Modeling provides curlV, gradP.
	MR3ii Measure $J_{\text{current\_sheet}}$ (planar approximation, $\delta J/J \sim 10\%$, $\delta B/B \sim 10\%$ or $\delta B \sim 1$ nT absolute, 0.1 nT relative, over $\delta Z \sim 0.5$ R_E) and incoming flows.	**MC3ii** P4 & P5 δZ-conjunctions provide $\delta B \sim 0.6$ nT absolute, 0.03 nT relative while P2 measures flows.
	MR3iii E field ($t_{\text{res}} = 10$ s) for non-MHD part of flow.	**MC3iii** E field measured at 4 vectors/s routinely.
	MR3iv Study > 10 events in each δX, δY, and δZ.	**MC3iv** Cross-tail, cross-sheet or tail-aligned separations: 320 substorms/yr. P2 (incoming flows) available during 160 of those. Simultaneity in δX–δY or δX–δZ observations (not required) is possible.
G4. Substorm coupling to local modes at 10 R_E	**MR4i** Cross-tail pairs to measure FLRs, KH and ballooning waves in B, P, V and E at $\delta Y \sim 0.5$–10 R_E, $t_{\text{res}} = 10$ s.	**MC4i** P3, P4, P5 measure B, P, V and E at separations $\delta Y \sim 0.3$–10 R_E, at $t_{\text{res}} = 3$ s or better.
	MR4ii Cross-sheet pairs to measure $J_{\text{current\_sheet}}$ (as before) as free energy for cross-field current instabilities at 6 Hz, on E field @ spin-plane (3D), B-field in 3D.	**MC4ii** P3 & P5 δZ-conjunctions measure sheet density ($B \sim 0.6$ nT absolute).
	MR4iii Study 10 substorms or more.	**MC4iii** 160 substorms/yr (P3, P5). P2 aligns and times flows for 64 substorms/yr.

SST detectors that will be affected by Sun pulse). $\delta B/B \sim 10\%$ requirements arise from the need to monitor the rarefaction wave (also the cross-tail current within $\delta J/J \sim 10\%$, given a $\Delta B \sim$B between probes at separation $\delta Z \sim 1$ R$_E$). In a minimum field of 10 nT this renders the absolute stability requirement of 1 nT.

THEMIS desires to measure at least a few solar wind-triggered and a few spontaneous onset substorms (assuming equal chances to observe each). At least 5 substorms should be observed in each probe conjunction configuration. This defines the baseline mission requirement. Given a 3–6 hr recurrence time for substorms (Borovsky et al. 1993), this necessitates 30 hrs of useful data in each year of conjunctions. THEMIS's orbit strategy accounts for >260 hrs of conjunctions in each year (Frey et al. 2008). Clear evidence that tail-aligned spacecraft equipped with THEMIS-like instrumentation can indeed monitor the progression of the incoming flows despite their $\delta Y \sim 1$–3 R$_E$ localization comes from fortuitous ISTP conjunctions during north–south arcs at late substorm recovery (Henderson et al. 1998; Sergeev et al. 2000).

While significant losses of useful events may occur due to plasma sheet fluctuations, lack of solar wind data, possible extreme event localization, and early evening/late morning substorms, the mission can easily satisfy the requirement to capture at least a handful of substorms from a tail-aligned vantage point and resolve the pressing question of substorm causality. Of those, a few high quality, clear and effective conjunctions will receive attention by a large number of people (like CDAW events).

The mission design is stable to the J2 terms of the geo-potential and sufficient fuel exists to counteract lunar perturbations. THEMIS is immune to the differential precession of the line of apsides between the high and low altitude orbits, because it relies on mean anomaly phasing to obtain tail alignments. Further information on how the THEMIS orbits, probe design, attitude, instruments, data rates and cadence satisfy mission objectives is presented in Sibeck et al. (2008).

2.2 Secondary Objective: Radiation Belt Energization

At storm main phase, MeV energy electrons are abruptly (1–4 hrs) lost; they reappear also abruptly at storm recovery with fluxes higher than prior to the storm (Fig. 6). This MeV electron flux increase represents the main electron flux increase of electrons during a storm. The observed *rapid* increase of MeV electron flux inside of geosynchronous altitude cannot be accounted for by the *relatively slow* diffusion of solar wind plasma. The "Dst effect" *alone* cannot account for this process either, since the electrons reappear at much higher fluxes than before the storm. Electron fluxes are therefore likely enhanced at $L = 11$ before being transported inwards. Daily variations of MeV electrons are modeled successfully under that assumption (Li et al. 2001), but it is unclear whether such an electron source is indeed present beyond geosynchronous altitude at storm recovery or whether local acceleration of inner magnetosphere cold/warm electrons by ULF or VLF waves may play a role (e.g., Friedel et al. 2002; Millan and Thorne 2007).

The instantaneous radial profile of the electron flux at constant μ and the transport process fully determine the evolution of the outer belt. But no single satellite traversing the equatorial radiation belt and its sources (i.e., L-values from 3.5 to 11) can measure the radial profile of the electron fluxes faster than once per ten hours, due to its orbital period. Low altitude (polar) satellites measure near-loss-cone fluxes and underestimate the true equatorial flux value which peaks at 90° at active times. Multiple satellites on eccentric, equatorial orbits are needed in order to provide repetitive cuts through the radiation belt. The satellites should be displaced sufficiently along their orbit. THEMIS's P3 and P4 probes are separated

Fig. 6 LANL satellite data from a storm on November 3, 1993 exemplify the rapid loss and reappearance of storm time electron flux at geostationary orbit at storm onset and rapid (1–4 hr) reappearance at recovery (Li et al. 1997)
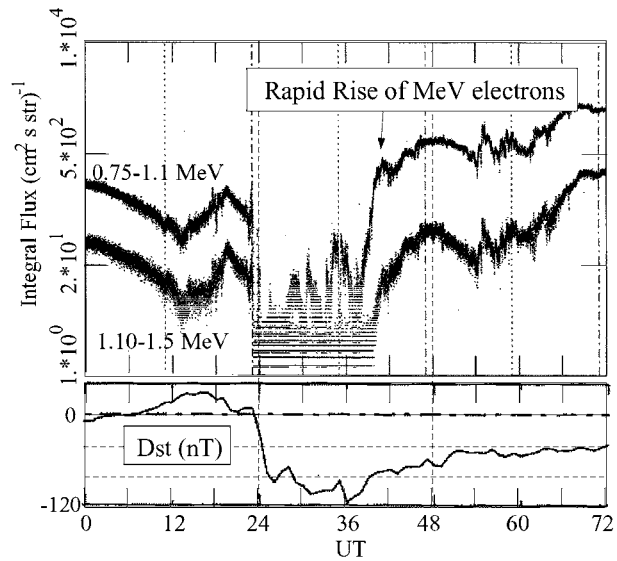
by several Earth radii along track when they traverse the radiation belts, due to their desired separation in mean anomaly for achieving tail science objectives. THEMIS's P5 probe is in a slightly different orbital period than sidereal. Probes P1 and P2 also traverse the radiation belts during the inbound and outbound passes. Together the five THEMIS probes traverse the inner magnetosphere from $L = 3.5$ to $L = 11$ with a median rate of recurrence of 3.8 hours. They can provide the needed radial profiles of the radiation belt electrons without any modification to the mission design. If the slope of the electron phase space density is inconsistent with a radially inward diffusion of killer electrons, THEMIS has the fields instrumentation to detect the presence and distribution of electromagnetic wave power to determine if such waves play a role in rapid electron acceleration at storm recovery.

2.3 Tertiary Objective: Upstream Processes

Observations near the equatorial magnetopause provide strong evidence for the predicted signatures of transient solar wind-magnetosphere coupling, namely fast flows (Paschmann et al. 1979) and flux transfer events (FTEs) (Russell and Elphic 1978). These may be either triggered by solar wind features (Lockwood and Wild 1993) or occur in response to intrinsic instabilities (Le et al. 1993). A number of other externally driven transient phenomena also contribute to the variations observed on single spacecraft. *Efforts to discriminate between the causes of magnetopause transients and determine the significance of each phenomenon to the solar wind-magnetosphere interaction have been hampered by several obstacles:*

First, observations near the L1 point or several 10 s of R_E off the Sun–Earth line are of limited use because solar wind features transverse to the Sun–Earth line are on the order of ∼20 R_E (Crooker et al. 1982; Paularena et al. 1998) and lag time uncertainties increase with distance (Collier et al. 1998). *Second*, foreshock and magnetosheath processes affect the magnetopause. These cannot be observed within the pristine solar wind (Fairfield et al. 1990; Thomas and Brecht 1988) and must be observed in place. Examples are: Hot flow anomalies transmitted across the bow shock (Völk and Auer 1974; Lin et al. 1996) and sheath (Paschmann et al. 1988; Sibeck et al. 1997); externally-driven, propagating slow shocks (Song et al. 1992) or standing slow shocks (Southwood and Kivelson 1995) in the

magnetosheath. *Third*, the significance of individual events depends upon their azimuthal dimensions. FTEs range from 0.5 to 5 R_E (Phan and Paschmann 1995). Events with similar features include solar wind/foreshock pressure-driven waves (Sibeck et al. 1989) or Kelvin-Helmholtz (Farrugia et al. 2001) waves.

Thanks to its unique Sun–Earth aligned probe conjunctions, THEMIS will overcome the aforementioned obstacles and determine the response of the coupled dayside solar wind-magnetosphere system to varying incident conditions. With particle and magnetic field instrumentation similar to that flown on AMPTE/IRM, THEMIS probes P1 and P2 will not only characterize the solar wind but also will determine its modification within the foreshock (Paschmann et al. 1988; Sibeck et al. 1989). Hundreds of hours of conjunctions will enable us to conduct statistics of event occurrence patterns and characteristics as a function of the solar wind conditions.

Further information of how THEMIS's instruments and orbits meet the mission requirements and address the science objectives, including preliminary results showing the efficacy of the THEMIS mission to perform its task is provided in Sibeck et al. (2008).

3 Mission Design

Minimum science closure can be achieved with four probes in one year of tail crossings. Inclusion of the fifth probe reduces risk and increases science return towards a baseline mission. Any of the inner probes have sufficient fuel reserves to replace either of the outer probes during the mission, but P5 was designated the "replacement probe". Science increase from the presence of the replacement probe allows probe pair measurements simultaneously in both *X* and *Y* GSM dimensions the first year (*Y* and *Z* dimensions the second year). Azimuthal separations are very desirable in both years in order to maintain an adequate baseline to determine the location and timing of the current disruption. Simultaneous radial and cross-sheet (*X* and *Z* GSM) separations await an extended mission.

The spinning probes ($T_{\text{spin}} = 3$ s) are designed to be dynamically stable even under worst-case scenarios (as demonstrated by fault tolerance analyses). A single-string probe design was further simplified by a minimal hardware complement, by inherent functional redundancy, strong instrument heritage and with the instruments and probe bus designed for graceful degradation. A probabilistic risk assessment and contingency analysis demonstrates that, with P5 ready to replace any other probe during the mission, even a single string design results in $> 93\%$ reliability for achieving the minimum mission. Redundancy is a key feature of any constellation of satellites and THEMIS is the first NASA mission to take advantage of it.

3.1 Probe Conjunctions

THEMIS was launched on February 17, 2007 and the probes were released on a highly elliptical, 14.716 R_E geocentric apogee, 437 km altitude perigee, 15.9 deg inclination, 31.4 hr period orbit by a Delta-II 7925 rocket from Cape Canaveral, with their line of apsides pointing at apogee towards the pre-midnight sector (Right Ascension of Perigee = 288.8 deg). The probes were checked out and placed in a stable, coast-phase orbit, traversing the dayside magnetosphere in a string-of-pearls configuration near their launch orbit. After instrument commissioning, the probes, initially named by their letters A–E, were assigned their target orbits and were designated a probe number based on their on-orbit performance (mainly antenna performance) as follows: B, C, D, E, and A were assigned constellation

positions P1, P2, P3, P4 and P5 respectively. In the initial part of the coast phase, concurrent with spacecraft and instrument commissioning (February–May 2007) the probe relative dispersion from the launch vehicle resulted in a C-DBA-E series configuration, with DBA clustered near each other at 100 s of km separation and C and E leading and training respectively by several 1000 s of km (Fig. 1). Magnetometer booms were deployed only days after launch but electric field antennas on TH-C (P2), TH-D (P3) and TH-E (P4) were deployed by mid-June 2007. Electric field booms on TH-B (P1) and TH-A (P5) were deployed in November and January respectively, i.e., after the placement maneuvers on those probes, in order to facilitate operations. After probe number assignment, it was decided that the probes with electric field antennas deployed during the coast phase would be maneuvered in the middle of the constellation, at small-scale separations, while the other two probes would become leading (TH-B) and trailing (TH-A). Inter-spacecraft separation was on the order of 100 km between inner probes and several 1000 s of km between the outer probes. Coast phase science in this optimal string-of-pearls configuration continued until the end of August 2007. Placement into the baseline orbits occurred between September and December 2007. Following on-orbit calibration and a period of bonus (non-baseline) coast-phase science, the probes were placed by December 4th 2007 into their final orbits in anticipation of the baseline mission. The baseline orbit strategy follows naturally from the requirements in Tables 1 and 4. Probe elements as function of year are tabulated in Table 5.

In the 1st tail season, P1 has apogee ∼30 R_E and a ∼4 day period, while probe P2 has apogee ∼19 R_E and a ∼2 day period. Once per 4 days these probes align near apogee and bracket the reconnection site. Probes P4 and P3 have apogees at 12 R_E and differ in their mean anomaly such that at apogee they are separated by ∼1 R_E. At or near apogee these probes routinely monitor the CD using the finite gyroradius technique. The third innermost probe (P5) has initially an apogee of ∼10 R_E: During the first tail season it has a faster-than-synchronous period, gaining 6 hrs/day along is orbit relative to P3, P4. Once every four days the inner probes cluster near apogee. Cross-tail separations between P3/4 and P5 range between 0.3 and 10 R_E and permit long wavelength studies of low frequency MHD waves. P5 is given an inclination change of 5° relative to P3,4. This affects the apogee conjunctions very little during the 1st tail season, when the argument of perigee (APER) is small; but creates a Z-separation of the inner probes in the 2nd tail season, when APER is large (note that the inner probes drift in APER by ∼90°/yr due to J2 terms).

The comprehensive THEMIS approach to solving the substorm problem calls for monitoring the nightside auroral oval with fast-exposure (1 s), low cost and robust white-light all sky imagers (ASIs) and high-time resolution (0.5 s) ground magnetometers to achieve faster than 3 s cadence measurements of the auroral break-up. A map of the sites is shown in Mende et al. (2008). The THEMIS Ground-Based Observatories (GBOs) cover a 12 hr local time sector, over the North American continent, from Eastern Canada to Western Alaska. ASIs provide a global view of the Northern Hemisphere aurora at unprecedented temporal and spatial resolution.

The THEMIS mission design optimizes substorm capture at probe conjunctions for the tail phases of the mission. A conjunction is defined as a four (or five) probe alignment within $\delta Y_{GSM} = \pm 2$ R_E, at the plasma sheet. Plasma sheet encounters are near-neutral sheet occurrences for the inner probes, P3,4,5 ($Z_{NS} = \pm 2$ R_E) but more relaxed for the outer probes, P1,2 since those probes' function is to determine Rx location using timing of boundary layer beams ($Z_{NS} = \pm 5$ R_E). Those major conjunctions occur once per four days, due to the orbit period of P1. Minor conjunctions are alignments between P2 and two inner probes. They recur once per two days (due to the orbit period of P2). When P1 is also available the minor conjunction becomes a major one. Daily conjunctions are those between P3, P4 (on a

Table 5 Probe elements as function of season (last 4 columns are predicts)

		Date: Release: 2007-02-18	Coast: 2007-07-15	Tail #1: 2008-02-02	Dayside #1: 2008-08-08	Tail #2: 2007-02-17	Dayside #2: 2007-08-13
P1	R_A [R_E, geocentric]	14.72	14.72	31.0	30.7	31.1	30.4
(TH-B)	R_P [km, alt]	437.	699.9	1275.	3824.	1402.	5418.
	INC [deg]	16.0	13.5	0.7	15.5	7.1	1.2
	RAP (=APER+RAAN) [deg]	288.8	302.9	312.	318.	322.	327.
	APER [deg]	319.6	344.2	270.	189.	354.	300.
P2	R_A [R_E, geocentric]	14.72	14.71	19.5	19.3	19.3	19.5
(TH-C)	R_P [km, alt]	437.	761.3	1976.	2613.	2039.	1594.
	Inc (deg)	16.0	13.5	5.6	0.9	13.6	11.
	RAP (=APER+RAAN) [deg]	288.8	302.9	314.	322.	331.	348.
	APER	319.6	344.3	3.0	94.	9.0	39.
sP3	R_A [R_E, geocentric]	14.72	14.72	11.8	11.7	11.6	11.6
(TH-D)	R_P [km, alt]	437.	720.5	2677.	3059.	4143.	4206.
	Inc (deg)	16.0	13.5	6.7	5.2	4.8	4.8
	RAP (=APER+RAAN) [deg]	288.8	302.6	322.	336.	341.	341.
	APER	319.6	343.8	20.	60.	99.	125.
P4	R_A [R_E, geocentric]	14.72	14.73	11.8	11.7	11.6	11.6
(TH-E)	R_P [km, alt]	437.	626.6	2677.	3059.	4079.	4270.
	Inc (deg)	16.0	13.5	6.1	4.7	4.1	4.6
	RAP (=APER+RAAN) [deg]	288.8	303.2	322.	336.	341.	341.
	APER	319.6	344.9	19.	59.	98.	122.
P5	R_A [R_E, geocentric]	14.72	14.70	10.0	10.8	11.7	12.9
(TH-A)	R_P [km, alt]	437.	881.9	2868.	3088.	3187.	3760.
	Inc (deg)	16.0	13.4	11.2	10.0	9.4	10.6
	RAP (=APER+RAAN) [deg]	288.8	302.4	318.	336.	343.	2.0
	APER	319.6	342.8	13.	55.	94.	118.

sidereal day period) and the ground-based observatories. By definition those occur at the nightside between 00:30 and 12:30 UT. Once per two days they include P2 and constitute minor conjunctions. Once per four days they include P1, P2 and P5 and constitute major conjunctions.

In preparation for 1st *year dayside observations* P5's apogee is raised to ~11 R_E with the same perigee, thereby increasing its period T_{P5} to 7/8 of $T_{P3,4}$. This has two advantages: First, it reduces the rate of differential precession of P5 relative to P3 and P4, in anticipation of the upcoming 2nd tail season. Second, it optimizes azimuthal separations between P5 and P4/5 at several R_E scales near the subsolar magnetopause to address the extent and lateral motion of boundary layer phenomena: Once per 8 days the subsolar magnetopause is encountered by all three inner probes with separations as close as 1–2 R_E, with P3 and P4 typically at the *magnetosheath* when P5 is at the *magnetopause*. During other periods of major, minor or daily probe conjunctions, separations between P5 and P3,4 at the magnetopause can be as large as 6 R_E or more.

For the 2nd *year tail season*, P5's apogee and mean anomaly are made identical to P3 and P4's. P5's inclination difference (5°) relative to P3/4 (achieved by a cost-effective maneuver in the 1st year), and orbit design considerations for a common inner probe APER (~90°) ensures a ~1 R_E difference in the *Z*-direction at apogee between P3,4 and P5. This permits studies of the thin cross-tail current during substorms (assuming a planar approximation) during the second tail season.

For the 2nd *year dayside season*, P5's apogee is increased to 13 R_E (same perigee as other probes), thereby increasing its period, T_{P5} to 9/8 of $T_{P3,4}$. During the 2nd year inner probe conjunctions at the magnetopause occur also once per 8 days, like the 1st year. There are, however, two differences: First, During the 2nd year P5 is a *magnetosheath* monitor at the subsolar region, whereas P3,4 are *magnetopause* monitors; Second, the average distance of magnetopause encounters is about 1 R_E further away from Earth than during the 1st year, which permits magnetopause observations in the pre- and post-noon sectors, further away from the subsolar point.

3.2 Inertial Location and Attitude of the Constellation

As the choice of a target date for center-tail observations moves from winter solstice into vernal equinox, the Sun–Earth line moves closer to the apsidal line near the equatorial plane and the maximum shadow duration of P1's and P2's near-Equatorial orbits increase. A given target date is characterized by the inertial location of the mission orbits' semi-major axis, whose longitude in inertial space is the least affected by lunar and J2 terms. The orbit inertial longitude is measured by the Right Ascension of Perigee (RAP), the sum of the argument of perigee (APER) and the right ascension of the ascending node (RAAN). RAP is fixed for each choice of a target center-tail date (e.g., it is 330 degrees for Feb-21 and moves a degree per day). Mission design seeks center-tail target dates that minimize shadows and maximize conjunctions. The choice of RAP = 312 deg for the 1st tail season was deemed optimal considering the entire end-to-end mission design, as it ensures > 188 hrs of tail-aligned conjunctions and < 3 hrs of shadows. This choice of inertial pointing of the constellation line of apsides in the sky determined the choice of our launch elements, such that the orbits drift into the desired inertial location in the sky by 1st year mid-tail (properly accounting for precession through the coast phase season). The RAP drifts by about 11°/year for P1, 22°/yr for P2 and 33°/yr for the inner probes. Thus, differential precession naturally limits the duration of useful conjunctions (and the mission lifetime) to approximately two years. Lunar perturbations affect mostly the outer probe inclinations and need to be balanced by

inclination change maneuvers. These, in addition to the orbit placement maneuvers, were the main drivers on probe fuel.

Additional considerations for the selection of the center-tail observation season were: (1) the substorm recurrence rate, which maximizes around equinoxes; (2) the dipole tilt, which affects neutral sheet hinging and reduces simultaneous residence in the plasma sheet at apogees of 10, 20, 30 R_E, by our near-equatorial probes; (3) the angle of the tail magnetic field to the nominal, near-ecliptic probe spin plane. This angle is desired to be $> 10°$ to enable computation of the spin axis electric field from the spin plane components, under the $\mathbf{E} \cdot \mathbf{B} = 0$ approximation, and increases away from solstice; (4) the ASI viewing conditions (cloud cover in Alaska and Western Canada reduces in late winter months with optimal viewing in mid-February); (5) the dark-sky duration at polar latitudes, which optimizes in mid-winter. Those considerations were satisfied by our choice of a tail season centered in mid-February.

The probes' nominal attitudes are nearly normal to the ecliptic plane. Driven by the desire for an efficient probe design (Harvey et al. 2008), only four thrusters are used in the probe design: Two co-aligned side thrusters, used for spin-up and spin-down, with thrust vectors located on a plane containing the probe center of gravity; two co-aligned axial thrusters, used for pulsed reorientations and for long duration, efficient orbit-change thrusts opposite to the spin axis. Axial thrusters are mounted at two bottom deck corners of the probes, pointing opposite to the spin vector. Therefore, the probes can thrust sideways and opposite to the spin axis but not along the spin axis. Large thrusts are nominally planned using the axial thrusters, after reorienting the probe spin axis along the desired deltaV direction. Once electric field booms are deployed reorientations are very costly in deltaV due to the large moment of inertia. Thus most large thrusts were executed during the orbit placement maneuvers prior to the electric field boom deployments. During the course of the baseline observation period, required thrusts by the inner probes are either on the ecliptic or near ecliptic-south. Thus the inner probes have to continue to point towards near-ecliptic north for the remainder of their lifetime, as they have since the early part of the mission and all through the coast phase. The outer probes, P1, P2, on the other hand, each have to perform one large inclination change maneuver prior to the second tail season, aimed at orbit corrections to lunar perturbations. Those maneuvers require thrusting near the ecliptic-north direction. This necessitates placing the outer probes with their spin axes pointing near ecliptic-south. Probes P1 and P2 were placed into an ecliptic-south attitude near the end of the placement maneuvers, in the Fall of 2007, and are expected to remain in that approximate attitude throughout the rest of their lifetime.

Finally, to ensure a large angle of the nominal magnetic field and the spin plane, the inner (outer) probe attitudes were tipped an additional 8° towards (away from) Sun on reference day of Feb 7, 2008. These attitudes also ensure that the electric field instrument spin plane spheres will not be shadowed by the probe body during most of the year, except for a period of several days at dawn and dusk when accurate electric field observations are less critical.

4 Instrumentation

The five spin-stabilized ($T_{\text{spin}} = 3$ s) THEMIS probes carry identical instruments that meet or exceed the requirements of the baseline science objectives. Table 6 summarizes the instruments and their specifications. A centralized parts-procurement, instrument development, quality assurance, safety and verification program resulted in an efficient production and integration of the THEMIS instruments. A production-line approach was utilized to increase

Table 6 THEMIS instruments

	Provider	Specifications	
FGM	TUBS& IWF	Stability	<1 nT/yr (0.02 nT/12 hrs)
	Auster et al. (2008)	Resolution	3 pT (digitization: 12 pT)
		Noise	10 pT/sqrt(Hz) @ 1 Hz
		Frequency	DC – 64 Hz[§]
ESA	SSL/UCB	Energy	i: 5 eV – 25 keV
	Carlson et al. (2008)		e: 5 eV – 30 keV
		$\delta E/E$	Inherent: i: $\sim$19%; e: $\sim$ 15%
			Transmitted: 35% (32 steps)
		g-factor, per anode	i: 0.875×10^{-3} cm^2 str keV/keV
			e: 0.313×10^{-3} cm^2 str keV/keV
		eflux, per anode	i: 10^3–10^9 eV/ (cm^2 s str eV)
			e: 10^4–10^{10} eV/ (cm^2 s str eV)
		Angular Res.	Inherent: e: (22.5° × 11.25°)
		Elev. × Azim.,	i: (SW: 5.625° × 5.625°max)
		FOV [deg]	Typical: 22.5° × 22.5°, 4π str
SST	SSL/UCB	Energy	i: 25 keV – 6 MeV
	Larson et al. (2008)		e: 25 eV – 1 MeV
		Energy steps	16 (transmitted)
		g-factor (closed/open)	i: 8×10^{-4}/0.1 cm^2 str
			e: 8×10^{-4}/0.1 cm^2 str
		eflux, per detector	i, e: 0.5–5×10^8 keV/ (cm^2 s str keV)
		Angular Res.	Inherent: 30° × 11.25°
		Elev. × Azim.,	Transmitted: 30° × 22.5°
		FOV	4 elevations ×16 azimuths
SCM	CETP	Frequency range	1 Hz – 4 kHz[§]
	Roux et al. (2008)	Sensitivity	0.8 pT/sqrt(Hz) @ 10 Hz
		Dynamic range	10^{-5}–1 nT/sqrt(Hz) [spectra]
EFI	SSL/UCB	Frequency range	DC–8 kHz[§]; AKR band: 100–300 kHz
	Bonnell et al.	Sensitivity	10^{-4} mV/m/sqrt(Hz) @ 10 Hz
	(2008)	Dynamic range	10^{-4}–10^2 mV/m/sqrt(Hz) [spectra]
		Time series:	±300 mV/m; 0.009 mV/m [DC coupled]
		range; resolution	±100 mV/m; 0.003 mV/m [AC coupled]
		Noise	3×10^{-6} mV/m (SpB); 3×10^{-5} mV/m (AxB)
		DC offset error	0.1 mV/m (SpB); 1 mV/m (AxB)
		Antenna lengths	50 m (12), 40 m (34), 7 m (56) tip-to-tip
GBO:	SSL/UCB	Sensitivity	< 1 kRayleigh
ASIs	Mende et al. (2008)	Resolution	> 250 pixels ASI dia.; 0.5° thumbnail
	Harris et al. (2008)	FOV	170 deg
		Spectral band	400–700 nm (white light)
		Cadence	3 s image rate / 1 s exposures
GBO/EPO:	UCLA	Noise	10 pT/sqrt(Hz) at 1 Hz
gmags	Russell et al. (2008)	Range/Resolution	±72,000 nT/0.01 nT
		Rate	2 samples/sec

[§]Nyquist

efficiency. A common Instrument Data Processing Unit (IDPU) housed all instrument electronics and interfaced with the Bus Avionics Unit (BAU) for data relay and instrument commanding. IDPU and BAU simulators developed early in the program allowed efficient parallel development of the probe and the instruments. The IDPU is described in Taylor et al. (2008). The BAU is described in Harvey et al. (2008). The FluxGate Magnetometer (FGM), measures the DC magnetic field up to 128 S/s and is described in Auster et al. (2008). The sensors were built by TUBS, and the electronics design and testing were performed by IWF. The flight electronics were implemented at UCB under a common-parts buy-and-make program. In-flight calibration was be performed by TUBS and UCLA. A magnetic cleanliness program was implemented jointly by UCLA and UCB. It encompassed parts selection and testing for DC and AC fields, modeling and compensation of solar panel and power system currents, propulsion system and SST magnets, i.e., the principal known offenders. Testing and verification took place at UCLA, UCB and JPL. Details of the magnetic cleanliness program are provided in Ludlam et al. (2008).

The ElectroStatic Analyzer (ESA), built at UCB to the recent heritage of the FAST ESA and the Cluster HIA instruments, measures ions and electrons between 5 eV and 25 keV. It is described further in Carlson et al. (2008). On-board moment computations on an FPGA permit subtraction of photoelectron fluxes and routine data collection and transmission of moments at spin period resolution. Careful ESA ground and in-flight inter-calibration, intra-calibration and absolute calibration are described in McFadden et al. (2008) and result typically in better than 10% accuracy moments.

The Solid State Telescope (SST), built at UCB to the recent heritage of similar instruments flown on the WIND and STEREO spacecraft, measures ions and electrons between 25 keV and >1 MeV. It consists of two units (heads) per probe, each unit measuring ions and electrons in two directions. Quadrupole fields resulting from matched and paired electron broom magnets reduce magnetic contamination. A mechanical attenuator results in a factor-of-100 increase in instrument dynamic range, which enables it to avoid saturation at the high fluxes near the inner edge of the plasma sheet, and have superior sensitivity at $\sim$30 R_E in the mid-tail and in the solar wind. The SST is described further in Larson et al. (2008).

The triaxial Search Coil Magnetometer (SCM) was built by CETP to the recent heritage of similar units flown on Cluster and Interball, and measures AC magnetic fields from $\sim$1 Hz to 4 kHz. The instrument is described in Roux et al. (2008). The signals from the three SCM sensor axes are pre-amplified in a highly integrated electronics module and then processed together with signals from the electric field instrument by a Digital Fields Board (DFB). The DFB processes the analog signal, digitizes the signal at high time resolution and produces a number of waveform and spectral data products available for triggers and memory storage and transmission. The board was designed by the University of Colorado and is described in Cully et al. (2008).

The three-dimensional Electric Field Instrument, EFI, consists of four spherical sensors, mounted on two pairs of 20 m and 25 m long Spin-plane Booms (SpB), built to the recent heritage of Cluster, and two axial tubular sensors, each $\sim$1 m long and mounted on an Axial Boom (AxB), a 3.5 m long stacer element, built to the recent heritage of similar units on FAST and POLAR. The boom electronics board in the IDPU controls the voltages on the sensors, preamp (ushers and guards), and braids while the aforementioned DFB conditions, digitizes and processes the signals and data products.

Figure 7 shows the THEMIS instruments in stowed and deployed configuration. Figure 8 shows the probe coordinate systems and the relative spin phase of the various instruments and in a deployed configuration. The FGM is on a deployable, articulated $\sim$2 m hinged boom and the SCM on a deployable $\sim$1 m boom (Pankow et al. 2008). The deployed booms
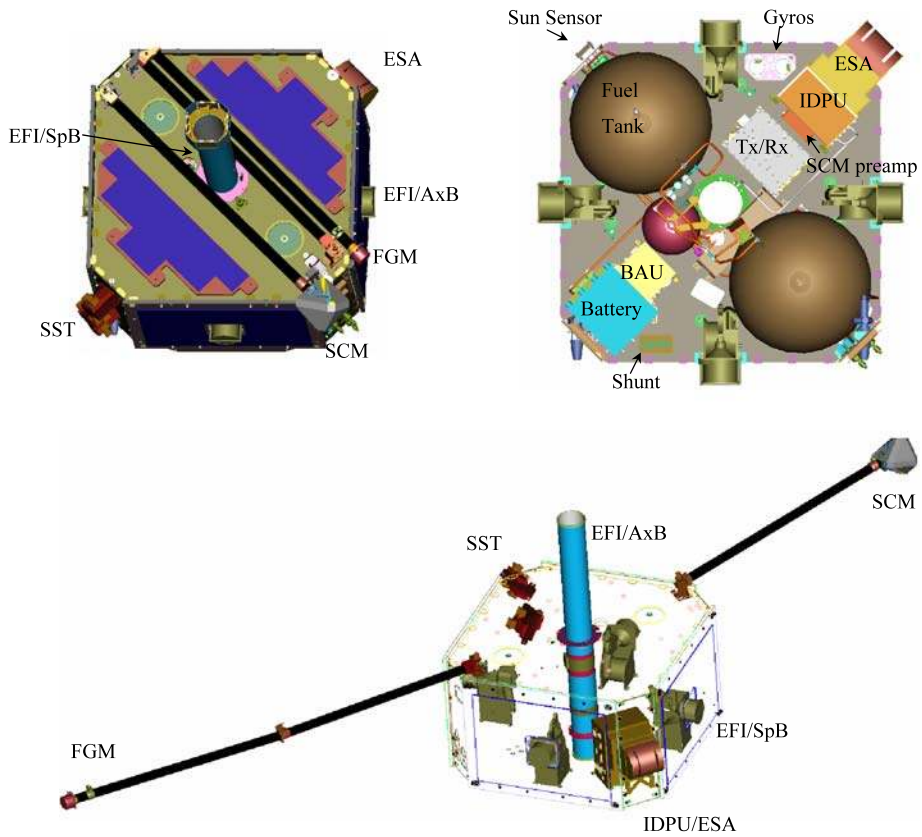
Fig. 7 (**a**) *top left*: Top view of THEMIS probe indicating locations of the instruments in a stowed config-uration; AxB is Axial Boom, SpB is Spin plane Boom; (**b**) *top right*: Internal instrument accommodation (**c**) *bottom*: Side view of THEMIS probe with magnetometer booms in deployed configuration, revealing instrument locations

are at an angle to the spin plane, such that even after the aforementioned 8° spin axis tip off the ecliptic normal, there is no boom shadowing of the solar arrays and thus stray currents and magnetic interference from the booms is minimal.

The Spinning Probe Geometric (SPG) coordinate system is also depicted in Fig. 8. The probe geometric axis, Z_{SPG}, was measured during environmental testing to be within 0.25° from the principal axis of inertia (which is the direction of the momentum vector, **L**). There-fore, the Spinning Sun-sensor L-vector (SSL) coordinate system, which is defined with the X_{SSL} axis along the field of view, the Sun sensor, Z_{SSL} axis pointing along the spin axis, or momentum vector **L**, and the Y axis completing the orthogonal system, is approximately (within much less than 0.25°) derived by a 135°rotation of the SPG system about the Z axis. The DSL system (not shown) is defined as a De-spun, Sun-pointing, L-vector system, such that Z_{DSL} is identical to Z_{SSL}, the $X_{DSL}-Z_{DSL}$ plane contains the Sun direction (X_{DSL} posi-tive towards the Sun), and the Y_{DSL} axis completes the orthogonal system. This is obtained from SSL to first order by a rotation opposite to the spin phase that elapsed since the last Sun crossing by the Sun sensor. Under nominal attitude, the inner probes (having a spin axis near ecliptic north) have a DSL system roughly along the GSE system (within 8°), whereas
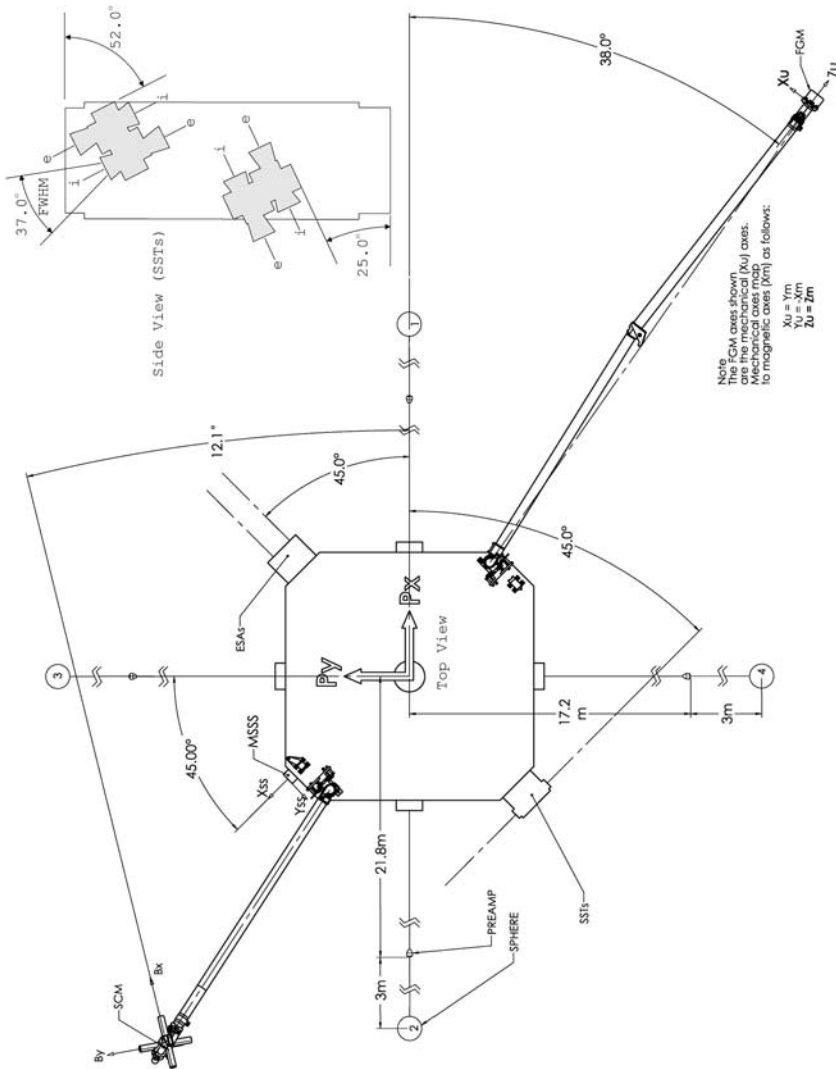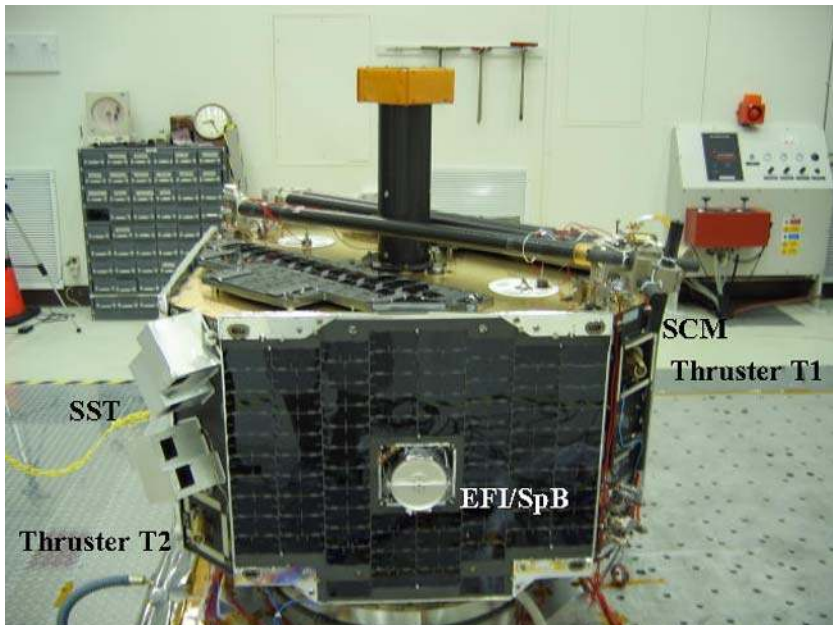
Fig. 8 Top view of THEMIS probe showing locations relative to each other and to the Sun sensor
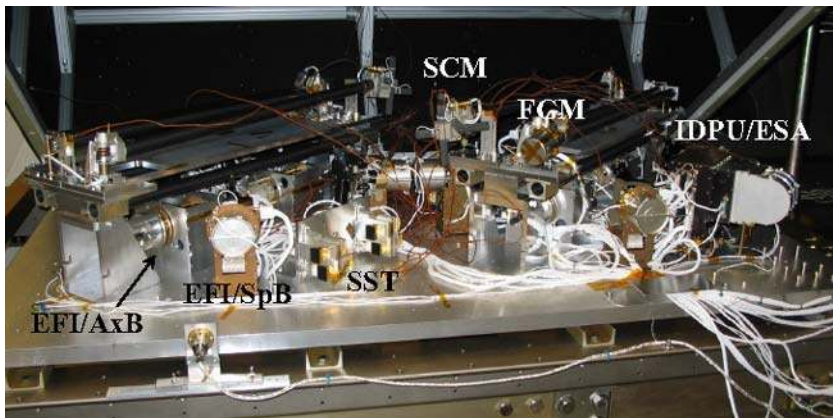
Fig. 9 THEMIS instrument suites FM2 (*left pellet*) and FM3 (*right pellet*), prior to undergoing thermal vacuum testing at the Space Sciences Laboratory, UCB

Fig. 10 THEMIS probe FM2 undergoing vibration testing at JPL. SSTs are covered by a thermal box, as in flight

the outer probes (having a baseline mission spin axis near ecliptic south) have a DSL system that is rotated 180°about the *X*-axis from GSE.

Figure 9 shows a picture of the THEMIS instruments undergoing environmental tests as a suite prior to integration with the spacecraft. Figure 10 shows an integrated probe during environmental testing.

The THEMIS ground-based observatory (GBO) instruments were designed to meet the mission requirements under minimum maintenance. The GBO systems were built at UCB

based on recent experience with the Automated Geophysical Observatories (AGOs) in Antarctica. Each station includes an auroral all sky camera imager (ASI), designed and developed at UCB based on commercially available components. A UCLA-provided GPS receiver card and magnetometer are also part of the integrated GBO design. UCLA magnetometers use a new electronics design, based on heritage from the UC-LANL, MEASURE, and SMALL ground magnetometer networks. Site installation at Canadian sites and data retrieval is done in collaboration with the University of Calgary. Existing magnetometer sites in Canada were reconfigured by the University of Alberta to produce data at 0.5 s resolution, and feed into, and be commensurate with, the standard THEMIS data flow. The THEMIS GBO program is described in Mende et al. (2008). The ASI imager is described in Harris et al. (2008). The GBO magnetometer stations are described in Russell et al. (2008), while Canadian-built THEMIS magnetometers and ancillary ground magnetometer datasets are described in Mann et al. (2008). The THEMIS team at UCLA produced and installed a network of mid-latitude stations to promote science education in rural schools. The way those tie into THEMIS's Education and Public Outreach program is described in Peticolas et al. (2008).

5 Mission Operations and Data Analysis

The THEMIS mission is operated by the Mission Operations Center (MOC) at the Space Sciences Laboratory, UCB (Bester et al. 2008). The MOC performs mission planning functions in accordance to science, flight dynamics, orbit and attitude determination, maneuver planning, commanding and state-of-health monitoring of the five probes, recovery of science and engineering data, data trending and anomaly resolution. Science operations comprise the generation of instrument schedules, data processing and archiving functions. The THEMIS ground systems are the Ground Station Network required for communications, the Mission Operations Center (MOC), the Science Operations Center (SOC) and the Flight Dynamics Center (FDC). The primary ground station for the THEMIS ground station network is the 11 m Berkeley Ground Station (BGS). Additional ground stations utilized are: Wallops Island (WFF), Merritt Island (MILA), Santiago Chile (AGO), and Hartebeesthoek (HBK) in South Africa. Recently, Universal Space Network stations in Hawaii (South Point) and Australia (Dongara) are coming on board to relieve the heavy load of routine contacts and provide backup capability. During the early part of the mission, the Deep Space Network and the TDRSS satellites have been also used for communications with the probes. Data are routinely transferred between various stations over secure network segments of NASA's IONet. The MOC, SOC, FDC and BGS are co-located at Space Sciences Laboratory, enabling efficient operations.

The probes are operated in store-and-forward mode. Transmissions are initiated by time sequence commands stored on-board. These commands are part of an Absolute Time Sequence (ATS) load generated individually for each probe with the Mission Planning System (MPS). ATS loads are uploaded up to a few times per week. Real Time Sequence (RTS) commands are also utilized when necessary. The command and control system for THEMIS is ITOS, the Integrated Test and Operations System, which allowed seamless transitioning of operations personnel from the Integration and Test phase pre-launch into flight operations post-launch.

Probe orbits were designed to meet science requirements using tools and training provided by NASA/GSFC. Specifically, the Goddard Trajectory Determination System (GTDS), a high-fidelity orbit integrator was ported into UNIX systems and was made

callable from an Interactive Data Language (IDL) higher-level data analysis and visualization language. This facilitated end-to-end mission design trades in order to optimize science (conjunctions) and reduce shadows and fuel. The General Maneuver program (GMAN), built also by NASA/GSFC and ported into the UCB mission design and mission operations tool-chest, permits finite-maneuver targeting functions with built-in propagation capability using GTDS. Calls to GMAN were also enabled from within IDL, such that a unified Maneuver Design Tool (MDT) encompassed the entire mission design effort calling interchangeably GTDS or GMAN depending on the fidelity and speed required. An IDPU engineering unit and two copies of the Bus Avionics Unit (BAU) unit equipped with an IDPU flight spare or an IDPU simulator are used to test commands before they are uploaded for execution in light, and are able to predict the vehicle behavior through special software. These "Flatsat" systems are used to test commands to instruments or spacecraft prior to execution in flight. This suite of programs and hardware provides an efficient and robust command generation and verification to meet science requirements, mission design requirements, operational requirements, and probe requirements in the pre- and post-launch phases.

Science operations are designed to accommodate an average of ∼750 Mbits per orbit, which is required from the probes. Instrument-specific loss-less compression is applied to reduce data volume by approximately a factor of two. Baseline primary science can be accomplished with routine data accumulation, which transitions from Slow Survey (SS) into a "Fast Survey" mode (FS) during conjunctions. Higher time resolution particles and fields accumulation is possible by burst mode collection, which is enabled by evaluating on-board trigger quantities.

Burst mode can be of two types: *particle* or *wave*. *Particle bursts* collect high-resolution distributions and low frequency waveforms. They are aimed at capturing the components of the global magnetospheric substorm instability (from -3 min to $+6$ min since burst trigger). They are triggered in the tail by dipolarizations, and in the dayside by density changes. Other trigger quantities are also possible. Since substorms occur ∼10% of the time (10 min collection/3 hr substorm recurrence time) which is similar to the occurrence rate of bursty flows (Angelopoulos et al. 1994, 1999) and current disruption in the region of primary interest ($X > -13$ R_E) our memory allocation of 10% of the conjunction time to particle bursts leads to full coverage of all surge intervals by this mode. *Wave* bursts are intended to capture the **E&B** field waveforms of the waves anticipated within the disruption region. Broadbanded low frequency waves occur nominally 10–20% of the bursty flow time (and proportionately less at higher frequencies). Memory allocation to wave bursts (10% of the particle burst time) results in waveform accumulation during most onset-related waves. Table 7 shows the data allocation per instrument assuming realistic compression levels, and Table 8 shows the resultant allocation per data collection mode. These apply for the inner probes. Outer probes have the same duration of particle burst per orbit as the inner probes and rely on additional contacts and compression to relieve the memory.

Upon receipt, and after quality checks and file statistics, automated file processing of the raw ("Virtual Channel" or VC) files takes place. The processing performs decompression, extracts housekeeping information, performs time-ordering and overlap-deletion, sorts by "Application Identifier" or "APID" code, containing data of an individual instrument or of an individual type and produces level zero (L0) files. These L0 APID files are generated as 24 hr files and can already be used directly for data analysis and visualization. However, further automated processing produces "Level 1" (L1) un-calibrated data files which are in machine-independent "Common Data Format" (CDF format), typically within an hour of downlink. L1 CDF files contain raw data from all instruments at the highest temporal resolution. Science team validated data are updated daily on the web along with standardized-format plots (.gif and .ps).

Table 7 THEMIS memory distribution, per instrument and mode, for the inner probes. Assumes realistic on-board compression (average compression of factor of 2)

P3/4/5	Mbits/	24	hrs			
Instrument	Slow Survey	Fast Survey	Particle Burst	Wave Burst	ACS	Total (Mbits)
FGM	1	6	14	0	2	24
SCM	1	17	19	9	0	46
EFI	2	31	25	18	0	75
SST	10	66	13	0	0	88
ESA	14	87	42	0	0	143
Volume	27	207	113	27	2	376

Table 8 Duration of various operational modes for the inner probes. Assumes realistic on-board compression (average compression of factor of 2)

T_orbit =	24	hrs	P3/4/5						Data Vol
S/C Mode	Rel. Allocation		Abs. Allocation		Hours	Seconds	Rate (bps)		(Mbits)
SS	50%	T_orb	12.5%	T_orb	12.0	43200	623		27
FS	50%	T_orb	11.3%	T_orb	10.8	38923	5324		207
PB	10%	T_fs	1.2%	T_orb	1.188	4277	26479		113
WB	1%	T_pb	0.0%	T_orb	0.012	43	629170		27
CAL	8.3%	T_orb	8.3%	T_orb	2.000	7200	261		2
									376

Data visualization and calibration is performed "on-the-fly" by routinely available IDL code, which uses the aforementioned L1 APID CDF files and instrument calibration files. The analysis code distributed also provides a Graphical User Interface (GUI) that allows users unfamiliar with command line IDL coding quick access to the data. The GUI is also accessible by IDL's Virtual Machine, which is free of charge. The IDL calibration and analysis code is disseminated to the community via the THEMIS web site; tutorials are routinely conducted at coI sites and during GEM or AGU meetings.

Further automated data processing performs standard calibration within hours of receipt, producing "Level 2" (L2) calibrated daily data files, also in CDF format. Those files do not require further calibration and can be read by any software that is able to access CDF files, such as Fortran, C, Matlab and IDL. Standard overview plots are also produced to facilitate data quality evaluation, and quick event selection, especially in conjunction with other missions. Plots, data, documentation and on-line tutorials are also available on the web (http://themis.ssl.berkeley.edu). Further description of the THEMIS science operations and data handling can be found in Phan et al. (2008).

6 Summary

THEMIS, the first NASA micro-satellite constellation, is a focused investigation to determine the onset and evolution of the macroscale substorm instability, a fundamental mode of mass and energy transport throughout Geospace. This primary objective drives mission design: resonant orbits of a minimum of four satellites bracket the reconnection and current disruption regions in the magnetotail to determine where the first energization during a

substorm occurs. A fifth probe is an on-orbit spare, which increases mission reliability and enables baseline science that far exceeds the minimum objective of substorm timing. The five-probe, 2 year baseline mission utilizes conjunctions with dedicated Ground-Based Observatories to monitor the auroral break-up and place the spacecraft observations in the context of global and local geomagnetic activity. Additionally, THEMIS's radial traversals of the radiation belts and their surroundings will address what causes the production of storm-time MeV electrons, and through its alignments in the dayside magnetosphere, will determine how the bow-shock and upstream processes affect the pristine solar wind and thus the solar wind-magnetosphere energy coupling. Understanding the ubiquitous substorm process, storm time electron energization and solar wind–magnetosphere coupling are essential for understanding and predicting space weather. While the currently operating Cluster mission and the upcoming MMS mission study in tetrahedral configuration local plasma boundaries from 100 s to 1000 s of km scales, THEMIS provides the necessary macro-scale vantage point, in the range of 1000 km–10 R_E, to study the global evolution of the magnetosphere during substorms. THEMIS is operating at a time when unprecedented coverage of the solar wind input is possible by WIND, ACE and STEREO. The THEMIS orbits are ideal for conjunctions with Cluster, other NOAA, DOE, NASA and international missions (such as GOES, LANL geosynchronous satellites, FAST and Geotail), and ancillary ground-based observatories (such as AMISR, SuperDARN, Sonderstrom and ULTIMA). THEMIS has an open data policy and readily provides data, documentation, plots, analysis software and training to the community at large, in order to maximize the benefit for the Heliophysics Great Observatory over the next decade.

References

A.T. Aikio et al., Characteristics of pseudobreakups and substorms observed in the ionosphere, at the geo-synchronous orbit, and in the midtail. J. Geophys. Res. **104**, 12263 (1999)

S.-I. Akasofu, *Physics of Magnetospheric Substorms* (Reidel, Dordrecht, 1976)

V. Angelopoulos et al., Statistical characteristics of bursty bulk flow events. J. Geophys. Res. **99**, 21257 (1994)

V. Angelopoulos et al., Magnetotail flow bursts: association to global magnetospheric circulation, relationship to ionospheric activity and direct evidence for localization. Geophys. Res. Lett. **24**, 2271 (1997a)

V. Angelopoulos et al., Multipoint analysis of a bursty bulk flow event on April 11, 1985. J. Geophys. Res. **101**, 4967 (1997b); also see correction: J. Geophys. Res., **102**, 211 (1997b)

V. Angelopoulos et al., On the relationship between bursty flows, current disruption and substorms. Geophys. Res. Lett. **26**, 2841 (1999)

V. Angelopoulos et al., Plasma sheet electromagnetic power generation and its dissipation along auroral field lines, J. Geophys. Res. (2001, in press)

G. Atkinson, The current system of geomagnetic bays. J. Geophys. Res. **23**, 6063 (1967)

U. Auster et al., Space Sci. Rev. (2008, this issue)

D.N. Baker et al., Neural line model of substorms: Past results and present view. J. Geophys. Res. **101**, 12975 (1996)

M. Bester et al., Space Sci. Rev. (2008, this issue)

W. Baumjohann et al., Average plasma properties in the central plasma sheet. J. Geophys. Res. **94**, 6597 (1989)

J. Birn et al., Flow braking and the substorm current wedge. J. Geophys. Res. **104**, 19895 (1999)

Bonnell et al., Space Sci. Rev. (2008, this issue)

J.E. Borovsky et al., The occurrence rate of magnetospheric-substorm onsets: random and periodic substorms. J. Geophys. Res. **98**, 3807 (1993)

C.W. Carlson et al., Space Sci. Rev. (2008, this issue)

M.R. Collier et al., Timing accuracy for the simple planar propagation of magnetic field structures in the solar wind. Geophys. Res. Lett. **25**, 2509 (1998)

N.U. Crooker et al., Factors controlling degree of correlation between ISEE 1 and ISEE 3 interplanetary magnetic field measurements. J. Geophys. Res. **87**, 2224 (1982)

C.M. Cully et al., Space Sci. Rev. (2008, this issue)

I.A. Daglis et al., "Fine structure" of the storm-substorm relationship: ion injections during Dst decrease. Adv. Space Res. **25**, 2369 (2000)

R.D. Elphinstone et al., Observations in the vicinity of substorm onset: implications for the substorm process. J. Geophys. Res. **100**, 7937 (1995)

D.H. Fairfield et al., Upstream pressure variations associated with the bow shock and their effects on the magnetosphere. J. Geophys. Res. **95**, 3773–3786 (1990)

D.H. Fairfield et al., Advances in magnetospheric storm and substorm research, 1989–1991. J. Geophys. Res. **97**(A7), 10865–10874 (1992)

D.H. Fairfield et al., Geotail abservations of substorm onset in the inner magnetotail. J. Geophys. Res. **103** (1998)

C. Farrugia et al., Viscous-type processes in the solar wind–magnetosphere interaction. Space. Sci. Rev. **95**(1/2), 443–456 (2001)

L.A. Frank, J.B. Sigwarth, Findings concerning the positions of substorm onsets with auroral images from the Polar spacecraft. J. Geophys. Res. **105**, 12747 (2000)

L.A. Frank et al., in *Proceedings of the International Conference on Substorms - 4 (ICS-4)* (Terra Scientific, Tokyo, 1998), p. 3

S. Frey et al., Space Sci. Rev. (2008, this issue)

Friedel et al., J. Atmospheric Sol. Terr. Phys. **64**, 265–282 (2002)

E. Friedrich et al., Ground-based observations and plasma instabilities in auroral substorms. Phys. Plasmas **8**, 1104 (2001)

S. Harris et al., Space Sci. Rev. (2008, this issue). doi:10.1007/s11214-007-9294-2

P.R. Harvey et al., Space Sci. Rev. (2008, this issue)

M.G. Henderson et al., Observations of magnetospheric substorms occurring with no apparent solar wind/IMF trigger. J. Geophys. Res. **101**, 10773 (1996)

M.G. Henderson et al., Are north-south aligned auroral structures an ionospheric manifestation of bursty bulk flows? Geophys. Res. Lett. **25**, 3737 (1998)

M. Hesse, J. Birn, On dipolarization and its relation to the substorm current wedge. J. Geophys. Res. **96**, 19417 (1991)

E.W. Hones Jr., The magnetotail: its generation and dissipation, in *Physics of Solar Planetary Environments*, ed. by D.J. Williams, AGU, vol. 558, 1976

E.W. Hones Jr. et al., Detailed examination of a plasmoid in the distant magnetotail with ISEE 3. Geophys. Res. Lett. **11**, 1046 (1984)

C. Jacquey et al., Location and propagation of the magnetotail current disruption during substorm expansion: analysis and simulation of an ISEE multi-onset event. Geophys. Res. Lett. **3**, 389 (1991)

J.R. Kan, A globally integrated substorm model: tail reconnection and magnetosphere-ionosphere coupling. J. Geophys. Res. **103**, 11787 (1998)

R.L. Kaufmann, Substorm currents: growth phase and onset. J. Geophys. Res. **92**, 7471 (1987)

Kennel, 1992, The Kiruna conjecture: The strong version, in *ICS-1 Proceedings*. ESA SP-335, 1992, p. 599

Larson et al., Space Sci. Rev. (2008, this issue)

G. Le, C.T. Russell, H. Kuo, Flux transfer events–Spontaneous or driven? Geophys. Res. Lett. **20**, 791 (1993)

X. Li et al., Multisatellite observations of the outer zone electron variation during the November 3–4, 1993, magnetic storm. J. Geophys. Res. **102**, 14123 (1997)

Li et al., Quantitative prediction of radiation belt electrons at geostationary orbit based on solar wind measurements. Geophys. Res. Lett. **28**, 1887 (2001)

Y. Lin, D.W. Swift, L.C. Lee, Simulation of pressure pulses in the bow shock and magnetosheath driven by variations in interplanetary magnetic field direction. J. Geophys. Res. **101**, 27251 (1996)

M. Lockwood, M.N. Wild, On the quasi-periodic nature of magnetopause flux transfer events. J. Geophys. Res. **98**, 5935 (1993)

M. Ludlam et al., The THEMIS magnetic cleanliness program. Space Sci. Rev. (2008, this issue)

A.T.Y. Lui, Extended consideration of a synthesis model for magnetospheric substorms. AGU Mon. Ser., vol. 64, 1991, p. 43

A.T.Y. Lui, Current disruption in the Earth's magnetosphere: Observations and models. J. Geophys. Res. **101**, 13067 (1996)

A.T.Y. Lui et al., A multiscale model for substorms. Space Sci. Rev. **95**, 325 (2001)

A.T.Y. Lui, J.R. Burrows, On the location of auroral arcs near substorm onsets. J. Geophys. Res. **83**, 3342 (1978)

A.T.Y. Lui et al., A case study of magnetotail current sheet disruption and diversion. Geophys. Res. Lett. **7**, 721 (1988)

L.R. Lyons, A new theory for magnetospheric substorms. J. Geophys. Res. **100**, 19069 (1995)

L.R. Lyons, Substorms: Fundamental observational features, distiction from other disturbances, and external triggering. J. Geophys. Res. **101**, 13011 (1996)

J.P. McFadden et al., Space Sci. Rev. (2008, this issue)

R. McPherron et al., Satellite studies of magnetospheric substorms on Aug 15th, 1968. J. Geophys. Res. **78**, 3131 (1973)

R.L. McPherron et al., Solar wind triggering of substorm onset. J. Geomagn. Geoelectr. **38**, 1089 (1986)

S. Mende et al., Space Sci. Rev. (2008, this issue)

Millan, Thorne, J. Atmos. Solar Terr. Phys. **69**, 362–377 (2007)

D.G. Mitchell et al., Current carriers in the near-Earth cross-tail current sheet during substorm growth phase. Geophys. Res. Lett. **17**, 583 (1990)

T. Nagai, Observed magnetic substorm signatures at synchronous altitudes. J. Geophys. Res. **87**, 4405 (1982)

T. Nagai et al., Substorm, tail flows, and plasmoids. Adv. Space Res. **20**, 961 (1997)

T. Nagai et al., Structure and dynamics of magnetic reconnection for substorm onsets with Geotail observations. J. Geophys. Res. **103**, 4419 (1998)

R. Nakamura et al., Flow bursts and auroral activations: Onset timing and foot point location. J. Geophys. Res. **106**, 10777 (2001a)

R. Nakamura et al., Earthward flow bursts, auroral streamers, and small expansions. J. Geophys. Res. **106**, 10791 (2001b)

S.-I. Ohtani, Earthward expansion of tail current disruption: dual-satellite study. J. Geophys. Res. **103**, 6815 (1998)

S.-I. Ohtani, Substorm trigger processes in the magnetotail: recent observations and outstanding issues. Space Sci. Rev. **95**, 347 (2001)

S.-I. Ohtani et al., Tail current disruption in the geosynchronous region, in *Magnetospheric Substorms*. AGU Mongr. Ser., vol. 64, 1991, p. 131

S. Ohtani et al., Radial expansion of the tail current disruption during substorms: A new approach to the substorm onset region. J. Geophys. Res. **97**, 3129 (1992a)

S.-I. Ohtani et al., Initial signatures of magnetic field and energetic particle fluxes at tail reconfiguration: explosive growth phase. J. Geophys. Res. **97**, 19311 (1992b)

Pankow et al., Space Sci. Rev. (2008, this issue)

G. Paschmann, G. Haerendel, N. Sckopke, E. Möbius, H. Lühr, C.W. Carlson, Three-dimensional plasma structures with anomalous flow direction near the Earth's bow shock. J. Geophys. Res. **93**, 11279 (1988)

Paschmann et al., Plasma acceleration at the magnetopause: evidence for reconnection. Nature **282**, 243 (1979)

K.I. Paularena et al., Solar wind plasma correlations between IMP 8, INTERBALL-1, and WIND. J. Geophys. Res. **103**, 14601 (1998)

Peticolas et al., Space Sci. Rev. (2008, this issue)

A.A. Petrukovich et al., Two spacecraft observations of a reconnection pulse during an auroral breakup. J. Geophys. Res. **103**, 47 (1998)

T. Phan et al., Space Sci. Rev. (2008, this issue)

T.D. Phan, G. Paschmann, The magnetosheath region adjacent to the dayside magnetopause, in *Physics of the Magnetopause*. AGU Monograph, vol. 90 (1995)

I.G. Richardson, S.W.H. Cowley, Plasmoid-associated energetic ion bursts in the deep geomagnetic tail: properties of the boundary layer. J. Geophys. Res. **90**, 12133 (1985)

I.G. Richardson et al., Plasmoid-associated energetic ion bursts in the deep geomagnetic tail: properties of plasmoids and the postplasmoid plasma sheet. J. Geophys. Res. **92**, 9997 (1987)

Roux et al., Space Sci. Rev. (2008, this issue)

Russell et al., Space Sci. Rev. (2008, this issue). doi:10.1007/s11214-008-9337-0

C.T. Russell, R.C. Elphic, Initial ISEE magnetometer results: magnetopause observations. Space Sci. Rev. **22**, 681 (1978)

J.C. Samson, Proton aurora and substorm intensifications. Geophys. Res. Lett. **19**, 2171 (1992)

E.T. Sarris et al., Location of the source of magnetospheric energetic particle bursts by multispacecraft observations. Geophys. Res. Lett. **3**, 437 (1976)

E.T. Sarris et al., Detailed observations of a burst of energetic particles in the deep magnetotail by Geotail. J. Geomagn. Geoelectr. **48**, 649 (1996)

R. Schodel et al., Rapid flux transport in the central plasma sheet. J. Geophys. Res. **106**, 301 (2001)

V.A. Sergeev et al., Triggering of substorm expansion by the IMF directional discontinuities: Time delay analysis. Planet. Space Sci. **38**, 231 (1990)

V.A. Sergeev et al., In situ observations of magnetic reconnection prior to the onset of a small substorm. J. Geophys. Res. **100**, 19121 (1995)

V.A. Sergeev et al., Steady magnetospheric convection: a review of recent results. Space Science Reviews **75**, 551 (1996a)

V.A. Sergeev et al., Detection of localized, plasma-depleted flux tubes or bubbles in the midtail plasma sheet. J. Geophys. Res. **101**, 10817 (1996b)

V.A. Sergeev et al., Multiple-spacecraft observation of a narrow transient plasma jet in the Earth's plasma sheet. Geophys. Res. Lett. **27**, 851 (2000)

I. Shinohara et al., Rapid large-scale magnetic field dissipation in a collisionless current sheet via coupling between Kelvin-Helmholtz and lower-hybrid instabilities. Phys. Rev. Lett. **87**, 095001 (2001)

K. Shiokawa et al., Azimuthal pressure gradient as driving force of substorm currents. Geophys. Res. Lett. **25**, 959 (1998a)

K. Shiokawa et al., High-speed ion flow, substorm current wedge, and multiple Pi2 pulsations. J. Geophys. Res. **103**, 4491 (1998b)

D.G. Sibeck et al., The magnetospheric response to 8-minute period strong-amplitude upstream pressure variations. J. Geophys. Res. **94**, 2505–2519 (1989)

D.G. Sibeck, K. Takahashi, S. Kokubun, T. Mukai, K.W. Ogilvie, A. Szabo, A case study of oppositely propagating Alfvén fluctuations in the solar wind and magnetosheath. Geophys. Res. Lett. **24**, 3133 (1997)

D.G. Sibeck et al., Space Sci. Rev. (2008, this issue)

G.L. Siscoe, H.E. Petschek, On storm weakening during substorm expansion phase. Ann. Geophys. **15**, 211 (1997)

J.A. Slavin et al., CDAW 8 observations of plasmoid signatures in the geomagnetic tail: An assessment. J. Geophys. Res. **97**, 8495 (1992)

P. Song, C.T. Russell, M.F. Thomsen, Slow mode transition in the frontside magnetosheath. J. Geophys. Res. **97**, 8295 (1992)

D.J. Southwood, M.G. Kivelson, Magnetosheath flow near the subsolar magnetopause: Zwan-Wolf and Southwood-Kivelson theories reconciled. Geophys. Res. Lett. **22**, 3275 (1995)

H.E. Spence, The what, where, when and why of magnetospheric substorm triggers. EOS **77**, 81 (1996)

Taylor et al., Space Sci. Rev. (2008, this issue)

V.A. Thomas, S.H. Brecht, Evolution of diamagnetic cavities in the solar wind. J. Geophys. Res. **93**, 11341–11353 (1988)

H.J. Völk, R.-D. Auer, Motions of the bow shock induced by interplanetary disturbances. J. Geophys. Res., 40-48, 1974

I. Voronkov et al., Shear flow instability in the dipolar magnetosphere. J. Geophys. Res. **104**, 17323 (1999)

J.R. Wygant et al., Polar spacecraft based comparisons of intense electric fields and Poynting flux near and within the plasma sheet-tail lobe boundary to UVI images: an energy source for the aurora. J. Geophys. Res. **105**, 18675 (2000)

Y. Yamade et al., Field-aligned currents generated in magnetotail reconnection: 3D Hall-MHD simulations. J. Geophys. Res. **27**, 1091 (2000)

E. Zesta et al., The auroral signature of earthward flow bursts observed in the magnetotail. Geophys. Res. Lett. **27**, 3241 (2000)